In situ TEM study of κ→β and κ→γ phase transformations in Ga2O3

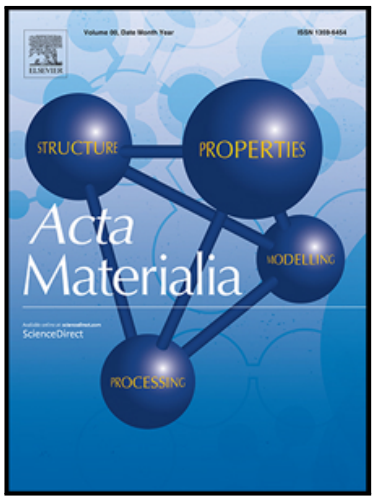

In situ TEM study of $\kappa \rightarrow \beta$ and $\kappa \rightarrow \gamma$ phase transformations in Ga_2O_3

I. Cora , Z.S. Fogarassy , R. Fornari , M. Bosi , A. Rečnik , B. Pécz

PII: S1359-6454(19)30750-5
DOI: https://doi.org/10.1016/j.actamat.2019.11.019
Reference: AM 15645

To appear in: *Acta Materialia*

Received date: 1 August 2019
Revised date: 7 November 2019
Accepted date: 7 November 2019

Please cite this article as: I. Cora , Z.S. Fogarassy , R. Fornari , M. Bosi , A. Rečnik , B. Pécz , In situ TEM study of $\kappa \rightarrow \beta$ and $\kappa \rightarrow \gamma$ phase transformations in Ga_2O_3, *Acta Materialia* (2019), doi: https://doi.org/10.1016/j.actamat.2019.11.019

In situ TEM study of κ→β and κ→γ phase transformations in Ga_2O_3

I. Cora[1], Zs. Fogarassy[1], R. Fornari[2,3], M. Bosi[3], A. Rečnik[4], B. Pécz[1]

[1]Centre for Energy Research, Institute of Technical Physics and Materials Science, Konkoly-Thege M. út 29-33., Budapest, 1121 Hungary

[2]University of Parma, Dept. of Mathematical, Physical and Computer Sciences, Viale delle Scienze 7/A, 43124 Parma, Italy

[3] IMEM-CNR, Viale delle Scienze 37/A, 43124 Parma, Italy

[4]Department for Nanostructured Materials, Jožef Stefan Institute, Jamova cesta 39, Ljubljana, Slovenia

Abstract

The temperature-driven phase transformation of metastable κ-Ga_2O_3 layers deposited on sapphire was studied by high resolution TEM. Annealing experiments up to 1000°C were performed either *in situ* in vacuum within the TEM or *ex situ* in ambient air. This allowed for the detection of the atomistic mechanisms at the basis of κ to β phase transition. In the case of *in situ* TEM observations we could even record in real time the atomic rearrangement. We provide in this paper the relevant crystallographic relations between original κ and new β lattice.

Surprisingly, the *ex situ* experiments demonstrated the additional formation of a γ-Ga_2O_3 intermediate phase at 820°C. The remarkably different behaviour between *in situ* and *ex situ* annealing experiments is explained in terms of ambient (ambient air or high vacuum) and heating rate.

An extensive investigation of γ-Ga_2O_3, also a metastable phase, showed that it has a cubic defect spinel structure (F$d\bar{3}m$) with disordered vacancies. Repeated observations of the

metastable γ-Ga_2O_3 after two months show that the vacancies tend to order, and that the vacancies are fully ordered after one year.

1. Introduction

Polymorphs of Ga_2O_3 are emerging as ultra-wide bandgap semiconductors [1] and are intensely investigated due to the recent advancements of growth technologies. Ga_2O_3 may be grown as large single crystals [1-3] and as thin film on homo- and heteroepitaxial substrates [4-13]. Applications of Ga_2O_3 range from alternative substrates for GaN epilayers, to very high power transistors [14-15] and solar blind deep-UV detectors [16-19].

Ga_2O_3 was thought to have six known polymorphs (α, β, γ, κ, ε and δ) [20-28] however the δ phase, first reported by Roy *et al.* [1], was recently suggested to be a mixture of ε and β phases [27]. Al- and Ga-oxides as earth metal-oxides show close structural relationship. Similar to alumina, α-Ga_2O_3 has a corundum structure (a=4.98 Å, c=13.44 Å, *R*-3*c*) with octahedrally coordinated Ga^{3+} atoms [20], but in contrast to alumina, this polymorph is metastable and transforms to the β phase above 500 °C [29-31]. β-Ga_2O_3 is the only stable phase among all the polymorphs. It has a monoclinic structure (a=12.23 Å, b=3.04 Å, c=5.8 Å, β=103.7°, *C*2/*m*), in which edge-sharing ribbons of GaO_6 octahedra run along the crystallographic b-axis. The ribbons are connected to corner sharing GaO_4 tetrahedra. The ratio of octahedrally and tetrahedrally coordinated Ga is 2:2. Its alumina analogue is the θ-Al_2O_3. γ-Ga_2O_3 is reported to have a defect spinel structure like γ-Al_2O_3. The Ga sites are only partially occupied, with varying ratio of octahedra and tetrahedra between 1.8:1 to 2.1:1 [27].

The orthorhombic κ polymorph of Ga_2O_3 has recently attracted much interest due to its spontaneous polarization of 0.23 C/m^2 [32-34] combined with ferroelectric behaviour [35]. κ-Ga_2O_3 is believed to be the second most stable after the β; it has an orthorhombic structure with 4H ABCB oxygen stacking [28,36]. It has been reported in nanometer-sized (110)-type

twin domains, where the 3 twin pairs together result a pseudo hexagonal lattice [28] (see Supporting Information **Fig. S1**). Therefore, this polymorph is often identified as disordered hexagonal ε in the literature. κ-Ga_2O_3 was grown successfully as single-phase layers on GaN, AlN, and β-Ga_2O_3, on c-sapphire and 6H-SiC by halide vapour phase epitaxy (HVPE), metal organic vapour phase epitaxy (MOVPE), atomic layer deposition (ALD), molecular beam epitaxy (MBE), plasma-assisted molecular beam epitaxy (PMBE), and pulsed laser deposition (PLD) [19,37-44]. The energy gap of about 4.6 eV of the κ/ε polymorph was measured by optical absorption and photoconductivity [19], while its electronic structure was very recently studied by XPS [45]. It can successfully be doped with Sn^{4+} and Si^{4+} to produce low-resistivity epilayers [40].

Not much is known about the transformations among the Ga_2O_3 polymorphs. The κ→β transition was first studied by Fornari *et al.* [46] and was reported to take place at temperatures above 850°C. However, in the same work, it was shown by differential scanning calorimetry (DSC) analysis that the transition is not direct, but occurs via intermediate steps, the first one taking place at about 650 °C while the transition to β goes rapidly to completion well above 850 °C.

The aim of the present work is to provide more insights into the atomic-scale processes taking place during the transformation of κ Ga-oxide. To this extent, different annealing experiments were carried out *in situ* within a transmission electron microscope (TEM) and *ex situ* on the same κ-Ga_2O_3 samples to identify individual phase transformation stages. Different kinds of TEM techniques, such as high resolution TEM (HRTEM), bright field (BF), selected area electron diffraction (SAED), nano beam diffraction (NBD), combined with image simulations, were used to explain the structural relationships at different stages of the transformation. In this work, we report on the first direct observation of crystallographic evolution during transition from the metastable κ- to the stable β-phase of Ga_2O_3.

2. Experimental

Epitaxial κ-Ga_2O_3 layers were grown by MOVPE in a cold-wall stainless steel chamber. The layers were deposited on (001) α-Al_2O_3 substrates at 650°C using trimethylgallium (TMG) and ultrapure water as reagents, while ultrapure H_2 was used as a carrier gas. Samples used for TEM investigations were about 250 nm thick (see Supporting Information **Fig. S1**). More details about the growth process are reported in [38].

Cross-sectional and plan-view samples for TEM studies were prepared by conventional ion-milling using Ar^+ ions (Technoorg Linda IV3 miller). Preparation details are given elsewhere [47]. The TEM samples were first examined by transmission electron microscope (Philips CM20) operating at 200 kV. HRTEM images, SAED and NBD patterns were acquired using a conventional 300 kV TEM (JEOL 3010 and JEOL 2010F) onto a Gatan Orius CCD camera. *In situ* heating experiments in the temperature range from room temperature to 1000 °C were conducted using a dedicated double-tilt TEM heating holder with Ta specimen spacers (Model 652, Gatan Inc. Pleasanton CA) in a conventional TEM (JEOL2100). *Ex situ* heating was conducted in ambient air within a Denkál 4-K/1100K furnace up to 820°C. Image and SAED simulations (defocal and thickness series with Multislice simulation) were calculated for the parameters of JEOL 3010 microscope using JEMS software [48]. The estimated thickness of the conventionally milled TEM specimens that are used for annealing was from ca. 10-15 nm (next to the hole) up to ca. 30-50 μm (at the edges of the disk).

3. Results

3.1. *In situ* annealing of κ-Ga_2O_3

Plan view TEM samples (sample #1) were examined *in situ* and annealed in the temperature range from RT to 1000°C (**Table 1**). Heating ramp was 2°C/min and annealing was performed under 10^{-6} Pa vacuum inside the microscope. The measured and documented

temperature data refer to the temperature of the heating holder and can deviate from the actual temperature in the region of interest (ROI) due to thermal resistances of sealing and the sample alone. The exact temperature of the examined area in the sample is probably lower, due to the low thermal conductivity of the materials between the heater and examined area (sample, glue, α-Al_2O_3) that may result in a certain temperature drop. TEM experiments were ~~not~~ aimed to identify the mechanism of transformations by assessing the reconstruction of polymorphs at the atomic scale, rather than determining the transition temperatures.

The data were compared to the DSC curve earlier reported by Fornari *et al.* [46] on the same material. Based on the DSC curves, a weak endothermic bend starting around at 650°C was identified, that was related to some kind of re-organization of the κ structure (**step #1**). After this initial step the crystallographic structure was seen to degrade quite rapidly, indicated by the absence of well-defined reflections in the X-ray diffractogram, which suggest a kind of "glass transition" at about 800 °C, consistently with the endothermic drop following the first inflection point of the DSC curves (**step #2**).

Finally, the exothermic transformation to β-Ga_2O_3 was reported to occur at 880-890°C [46] (**step #3**).

In our heating experiments we used this preliminary experiment as reference of where to expect the transitions reported in [46]. In the first heating range (corresponding to the **step#1** of [46]) we documented a very slow motion of the grain/twin boundaries, along with the movement of anti-phase boundaries/zones accompanied by the enlargement of domain sizes in the plan view samples. These structural changes probably correspond to the first weak endothermic bend at 650°C. Sizes of the domains are between 5-35 nm. Further heating of the samples resulted in a sudden phase transformation at 950-960°C: the κ-phase entirely transformed into the stable β-phase except in the rim of the specimen, probably due to the lower local temperature.

The orientation relationship between the resulting β- and the initial κ-phase was examined by SAED and HRTEM. The ABAC stacking direction of oxygen sublattice is parallel to [001] in the κ phase. Here chains of edge-sharing octahedra alternated with corner-sharing tetrahedra are running along the a-axis (**Fig. 1**). The monoclinic β-Ga_2O_3 has a pseudo cubic ABC oxygen stacking. Edge-sharing octahedra run along the b-axis. There are 4 directions of close packed layers in β phase (corresponding to the {111} planes in *ccp* structures, with 70.4° between them), *i.e.*: $\{\bar{2}01\}$, {101}, $\{3\bar{1}0\}$ and {310} monoclinic planes. Since it is a monoclinic structure, Ga ordering between the closed packed oxygen layers are different in these 4 directions (**Fig. 1**). Any of the *ccp* layers can translate parallel into the {001} *hcp* layers of the κ-phase. The close-packed stacking directions of the O-sublattices are related to the corundum substrate, following OR1 (orientation relationship): $\{001\}_{\alpha\text{-}Al2O3} \parallel \{001\}_{\kappa\text{-}Ga2O3} \parallel \{\bar{2}01\},\{101\},\{3\bar{1}0\},\{310\}_{\beta\text{-}Ga2O3}$ (**Table 2**).

We documented the orientation relationship between the β and the κ phases on BF, SAED (**Fig. 2**) and HRTEM images (**Figs. 3 and 4**) from the plan-view sample. **Fig. 2** shows SAED patterns of the two polymorphs in two orientations. The tilting angles between the two projections (**Fig. 2A and Fig 2B**) were: Δx=+6.2° and Δy=+5.8°. This allows us to reconstruct the orientation/structural relationship between nutrient κ and newly generated β-phases: $\{310\}_{\beta\text{-}Ga2O3}$ plane is parallel to the $\{001\}_{\kappa\text{-}Ga2O3}$ (**Fig. 2C and 2D**). **Fig. 3** shows the HRTEM image of the interface in [001] zone axis of κ-phase. On FFT image from area B $\bar{2}04$ and 510 reflections of the β-phase are in the same orientation with orientation relationship OR2 (**Table 2**): $[2\underline{1}0\bar{1}]_\beta \{\bar{2}04\}_\beta \parallel [001]_\kappa \{010\}_\kappa$.

During and after the heating of sample-we also found traces of the cubic γ-phase. On FFT of **Fig. 4** from area C three peaks appear at 2.5 Å 60° from each other, that could correspond to the 220-type reflections in the $[1\bar{1}1]$ zone axis of γ-phase, since cubic O-stacking in the γ-

phase is parallel to <111> directions. Honeycomb-like features on HRTEM also support this interpretation. Orientation relationships between the 3 phases are OR3 (**Table 2**): $[2\underline{1}01]_{\beta}$ $\{\bar{2}04\}_{\beta}$ || $[001]_{\kappa}$ $\{010\}_{\kappa}$ || $[1\bar{1}1]_{\gamma}$ $\{220\}_{\gamma}$. No additional phases nor amorphous pockets were detected by TEM. With reference to the DSC data of ref. [46], we could only confirm the **step#1** and **step#3**, the sharp exothermic transformation, but we have not observed an amorphous intermediate state.

β-phase shows several twin boundaries parallel to $(\bar{1}00)$, where layers parallel to $(\bar{2}01)$ continue in the layers parallel to the (101), that can form easily during the very fast expansion of the β-phase.

Cross-sectional TEM samples

As for the case of plan-view experiments, *in situ* experiments were also performed ~~also~~ on cross-sectional specimens (**Table 1**). These experiments were rather complicated and not always successful. All samples were heated up to 600°C in larger steps (50°C/5 min), then we applied different ramps to each sample: 5°C/min in sample #2, 3°C/min in sample #3 and the slowest 1°C/min ramp in sample #4. We observed phase transformations at 940°C and 980°C. Again, the transition temperatures generally higher than those reported by DSC reflect probably the low heat conductivity of experimental setup, while the gap from 940°C to 980°C reflects its thermal inertia. The transformation suddenly started and was very quick in two samples with higher heating rate. In sample #3 we could record the transformation in real time at 20K magnification (**Video 1**). The new phase nucleated in the thicker part of the sample then it expanded in lateral direction up to the middle of the observation field. The new phase was identified as the thermodynamically stable β-phase. We repeated the same experiment with sample #4, applying the slowest heating ramp. In the range of 500 °C to 850°C the heating rate was 1°C/min, while above 850°C with using the same heating rate we kept the sample at a fixed temperature for 10 minutes at intervals of 20°C. The

transformation started at about 950°C, but it was slower than observed in sample #3, presumably because of the lower heating speed that did not generate any temperature overshooting by the temperature controller. The transformation started in the middle of the layer as well, and spread laterally (**Video 2 and 3**), self-sustained by the exothermic heat of transition. **Figure 5** (taken from the movie) shows the orientation relationship between the two phases. The kinetically driven phase transformation from 4H κ- to monoclinic β-phase with 3C O-sublattice is clearly topotaxial, with O-sublattice retaining the same directions, as recently reported for the *hcp-ccp* phase transition in spinel [49]. During the reconstructive transformation of oxygen sublattice from 4H (ABCB) hexagonal to 3C cubic (ABC) not all the oxygen layers need to shift (**Fig. 6**); 4 layers out of 12 run coherently between the two phases, while the others in-between are reconstructed. The new phase expands laterally with a zig-zag interface, since the transformed oxygen layers (which require the stacking shift from A to B) are left a bit behind those which proceed coherently. The transformation of Ga_2O_3 film proceeds in the mid of the epilayer, then it slows down and stops leaving about 20-50 nm of κ-phase at the top and bottom of the film. The transformation front parallel to $(001)_\kappa$ and $(111)_\gamma$ is more stable and sharp, therefore the transformation requires more energy in order to advance in vertical direction, and thus it is slower in that direction. The fact that the transformation starts in the middle of the epilayer could be explained by considering the interface energy. Since the κ-phase has lower interface energy with corundum than the β-phase, the interface stabilizes its structure to higher temperatures. The transformation from κ- to β-phase results in energy release that is proportional to the volume of transformed material. This transformation energy could be comparable with interface energy difference between the two phases in such small thickness. Detailed DFT study could confirm this assumption.

Along with the O-sublattice, Ga positions are totally changed as well, with different patterns of Ga ordering taking place in the new born phase. As mentioned above, there are

four orientations of *ccp* oxygen layers in the β-phase. Consequently, Ga ordering between the *ccp* oxygen layers are different in the 4 directions. Any of the 4 closed packed layers could be parallel to the {001} *hcp* layers of the κ-phase.

Figure 7 (A-C) from the sample #2 with the highest heating rate shows that β-phase formed from κ in the middle of the layer. **Figure 7D** of the same sample shows where two differently oriented β-domains formed from κ-phase meet. The orientation relationship between them are the following OR4 (**Table 2**): $[001]_{\kappa}$ $\{001\}_{\kappa}$ || $[\bar{2}\underline{1}0\bar{1}]_{\beta1}$ $\{3\bar{1}0\}_{\beta1}$ || $[2\underline{1}01]_{\beta2}$ $\{310\}_{\beta2}$. In both cases the close-packed oxygen layers are parallel, however the stacking direction is the opposite.

On the top of the remained κ (**Fig. 7**) and in small lateral segments on the interface between κ and β also cubic γ-phase was formed with the following OR3 (**Table 2**): $[001]_{\kappa}$ $\{200\}_{\kappa}$ || $[2\underline{1}01]_{\beta}$ $\{510\}_{\beta}$ || $[1\bar{1}1]_{\gamma}$ $\{2\bar{2}4\}_{\gamma,}$ while the stacking direction of oxygen is the same as in κ- and β-phases. 222-type peaks on XRD pattern from Fornari *et al.* [46] confirm the presence of γ-phase first transformed from κ-phase. However, during the transformation (**Video 2 and 3**) from κ to β we did not observe any trace of the γ-phase at the interfaces, it appeared only when the transformation was slowed down and after the annealing. We will discuss about the γ-phase in detail later.

3.2. *Ex situ* annealing of κ-Ga_2O_3

A TEM cross section lamella (sample #5) was annealed *ex situ* in ambient air up to 820°C for 15 minutes (**Table 1**). The heating rate between 500 and 820°C was ~10°C/min while the subsequent cooling rate was ~5°C/min. After annealing the lamella was studied by TEM. The BF image (**Fig. 8**) shows the transformation in its frozen state. As for the *in situ* experiments, the new phase expanded laterally. In the thinnest part, on the edge of the thinned TEM specimen (right next to the hole) islands of the new phase of about 40 nm x 10 nm appears in the middle of the layer. In the thicker part, the phase consists of ca. 50 nm wide elongated

slabs. Acquired tilt series of diffraction patterns (**Fig. 8**) revealed that this phase is cubic γ. The slabs are the {111}-type twins of each other (**Fig. 8**). Formerly, Cora *et al.* [28] identified a buffer at the interface between sapphire substrate and the κ-layer that was suggested to be made of γ-Ga_2O_3. It seems here that the transformation from κ to γ upon annealing indeed occurs within the layer rather than at the interface. It would seem that if the annealing is not sufficient to trigger the κ → β transformation, *i.e.* in absence of the exothermal heat, only a partial transformation to the metastable γ can take place. In the case of *in situ* experiment, the available heat was larger (higher T), and the β could form directly. Towards the end of the transformation, when approaching the interface and external surface, heat is dissipated more promptly and the exothermic heat alone does not grant the formation of the stable β phase, but is sufficient for the formation of γ-islands. We must also consider that the *ex situ* annealing was in O atmosphere, which might have a stabilizing action towards the γ phase in form of thicker slabs. This transformation could be somehow related to the **step#2** detected by DSC around 800°C [46].

3.3 Structure of the cubic γ phase and the transformation interface between κ and γ

In the ICSD database five Ga-oxide structures [27, 50-52] are reported as cubic γ-phase. All of them are classified as a defect spinel structure with the $Fd\bar{3}m$ space group symmetry. In the $MgAl_2O_4$ spinel structure the O-sublattice has a close-packed cubic ABC stacking. Al and Mg atoms are located in the 16d (with octahedral coordination) and the 8b (with tetrahedral coordination) Wyckoff-sites with 1.0 site occupancy resulting a cation:anion ratio of 3:4. In the published cubic γ-Ga_2O_3 structures all of the possible octahedral and tetrahedral sites (8a, 8b, 16d, 16e, 48f) between the oxygen close-packed layers are filled with a lower probability/occupancy (see Supporting Information **Fig. S2**), resulting vacancies. These published structures assume face sharing of occupied interstices, which is very uncommon among oxides. Among Al-oxides the γ-Al_2O_3 has a defect spinel structure ([53-55], the same

structure being referred to also as sigma [56]). Since in Al_2O_3 (as Ga_2O_3) the cation:anion ratio is only 2:3, vacant interstices also exist in the spinel structure. Two different Al-oxide structures are reported in the ICSD: 1) with vacancies in the 8b site with 0.667 site occupancy factor (s.o.f.) [55] called "*8b* structure" and 2) with vacancies in the 16d site with 0.833 s.o.f. [53-54,56] called "*16d* structure" that give a 2:3 ratio of Al/Ga:O. If vacancies are disordered, the s.g. symmetry remains $Fd\bar{3}m$. We simulated two cubic Ga-oxide structures in analogy with the two Al-oxides (see Supporting Information **Fig. S2**).

Experimental SAED, NBD patterns and HRTEM images were acquired of the γ-phase from the sample #5 annealed *ex situ* in ambient air up to 800°C, and from the sample #4 heated up to 950°C *in situ* within the TEM under vacuum.

SAED and NBD patterns and defocus series of HRTEM images for different thicknesses were simulated using JEMS software package [48] for all of the Ga-oxide structures from ICSD and for the two constructed Ga-oxide phases (as γ-alumina analogues) in $[11\bar{2}]$ and [110] zone axis. Diffraction patterns were calculated up to 33 nm sample thickness applying dynamical approach. For HRTEM images we used multislice image simulations. Simulated images and patterns for Ga-oxide structures from ICSD differ significantly from the measured data. Therefore, we compared the experimental data with the simulated ones for the two constructed Ga-oxide phases.

Dynamical scattering is very robust for spinel structure. Argand-plots showed that in the $[11\bar{2}]$ and [110] zone axis (z.a.) only for the first few nm thickness the scattering is proportional to the kinematical ones, whereas for thicker samples dynamical approach should be applied. Tilt series of NBD were acquired of γ-Ga_2O_3 from sample 3 and we compared the simulated diffraction intensities with the experimental ones (**Fig.** 9) in [110] zone in order to check their reliability. The intensity ratio as function of thickness between the three strongest

reflection (004, 440, 222) in [110] z.a. and the intensity ratio of 204 and $3\bar{1}1$ in $[11\bar{2}]$ z.a. (see Supporting Information **Fig. S3**) show significant difference between the two possible structure, *8b* and *16d*, and can help to identify which of the two constructed lattices realistically represents our γ structure. **Table S1** (see Supporting Information) shows the measured intensities of reflections in [110] z.a. and the simulated ones for different thicknesses of the *8b* and *16d* structures. Simulated intensities of 16d structure do fit the experimental ones in the thickness range of 9-14 nm. Slight differences could be caused by a slight misalignment of the zone axis. Based on simulations, the maximum value of misalignment could be around 0.1-0.3°. For the *8b* structure the calculated and experimental intensities match around 22 nm. In order to decide which model (*8b* with 22nm or *16d* with 9−14 nm) fits to our γ structure we examined the ratio of 204 and $3\bar{1}1$ reflection intensities in $[11\bar{2}]$ z.a.. The experimental measured value of $I_{3\text{-}11}/I_{204}$ is 4.92. This value corresponds to 12 nm thickness in the case of *16d* structure, which is in agreement with the estimated thickness value from **Table S1** (see Supporting Information). In the case of *8b* structure ratio of 4.94 corresponds to a 9 nm thickness, which shows a remarkable discrepancy with the estimated thickness value (22 nm) from **Table S1** (see Supporting Information). We also simulated HRTEM images (see Supporting Information **Fig. S4**) for the two hypothetical γ structures and the κ phase right next to them in order to decide between the 22 nm thick *8b* or 9−14 nm thick *16d* model. Simulated HRTEM images with thickness of 8−15 nm are significantly more accurate than images with thickness of ~22 nm. Therefore, we are led to conclude that the cubic γ phase has a defect spinel structure with 0.83 occupancy in the 16d Wyckoff site. We could not refine exactly the occupancy of the two cation sites, since smaller differences in occupancy result differences in intensity and phase smaller than differences in intensities caused by error of our experimental setup. The thinnest part of the γ phase from sample #5

was studied by HRTEM and multislice image simulation that well agree with the 16d structural model (**Fig. 10**).

SAED patterns of the γ-phase from the sample annealed *ex situ* (sample #5) were repeated two months after and one year after the heating experiment, respectively. After two months we acquired diffraction patterns from [11$\bar{2}$] and [12$\bar{3}$] zone axis. While one of the 110-type reflections remained forbidden, the 1$\bar{2}$0 appeared in [12$\bar{3}$] zone axis (z.a.) (**Fig. 11**). We constructed 16 different structures which fulfil this extinction rule. In all structures, vacancies are ordered in stripes parallel to one or two <1$\bar{2}$1> directions (see Supporting Information **Fig. S5**). Unfortunately, because of the error in intensities caused by possible misalignment and the nano-twinning of the material, it made no sense to compare simulated intensities of constructed structures with the experimental data. Diffraction experiments repeated after one year from the original annealing, showed that extra reflections (110 as well) appeared on SAED patterns violating the *F*-centering resulting in a *P*-type cell. This means that vacancies are totally ordered after one year and nano-twins were formed in a consequence of vacancy ordering. The presence of nano-twins associated with the ordering of vacancies make the crystallographic study very difficult in the case of spinel structure type. The interface between κ and γ was studied after the transformation (**Fig. 12-13**). The interface is running zigzag in lateral direction while it has a sharp edge parallel to $[001]_{\kappa}/[111]_{\gamma}$. On the zigzag lateral interface the octahedral layer of κ phase meets the pure octahedral (kagome) layer of γ phase and so do the mixed layers (**Fig. 12 and Fig. 13A**). At the interface, oxygen vacancies possibly form in several (but not in all) layers, since ABC stacking meets with ABAC hexagonal stacking. On the interface parallel to $(001)_{\kappa}/(111)_{\gamma}$ there is a two-layer thick transition zone (one octahedral and one mixed, tetra-, octahedral layer) between the two structures (**Fig. 13B**). As we have discussed above, the rate of the transformation in lateral direction is much faster than in the perpendicular direction. **Fig. S6** shows more interfaces

among the three polymorphs. Interface between γ and β is smooth, since the oxygen atoms have identical stacking. The interface between β and κ however, is wavy, due the changes in the stacking. Wavelengths of the waves correspond to the structure shown of **Fig. 6**.

4. Conclusions

In the present study different TEM-based methods were applied to investigate the phase transition consequent to thermal annealing of orthorhombic κ-Ga_2O_3 epitaxial films in two different conditions: *in situ* under vacuum up to 950 °C and *ex situ* in air up to 850 °C. This allowed to understand the evolution of the κ→β phase transformation, which indeed includes different steps. With *in situ* TEM experiments we observed that the **step#1** corresponds to slow motion of the antiphase and grain/twin boundaries within the κ-phase at about 650 °C, with corresponding enlargement of domain sizes up to ~35 nm. When the temperature is further increased up to 950 °C a sudden and quick κ→β exothermic transformation occurs, which we identify as **step#3**. The speed of the κ→β transition was seen to depend on the sample heating rate. Quite surprisingly, we found that β first nucleates in the middle of the epilayer and then it extends laterally and vertically. The original and new polymorphs share the same oxygen stacking direction, and four oxygen layers out of twelve run coherently across the interface between 4H (ABCB) κ and 3C (ABC) β phases. The newly born β grain expands with a smooth and stable interface in $(001)_\kappa$ direction (kind of singular surface) so that ultimately the vertical expansion is much slower than the lateral (zigzag) one. The phase conversion stopped some 20-50 nm from the film surface and substrate interface, which we tentatively explained in terms of surface energy.

The intermediate **step#2** was identified only in samples annealed *ex situ* in air. SAED patterns and HRTEM images proved that, in addition to the native κ, a new γ-phase was generated, in form of *ca*. 50 nm wide elongated slabs extended towards the thicker part of the

sample. It seems that a partial pressure of oxygen and higher heating rate are necessary conditions for γ phase to form upon thermal treatment.

A detailed investigation of the γ phase, based of experimental SAED and NBD patterns, and HRTEM images with relevant simulations, suggested that the first formed γ-Ga_2O_3 has a cubic defect spinel structure ($Fd\bar{3}m$), most probably of *16d*-type, with disordered vacancies, analogous to γ-alumina. However, this structure is very prone to ordering. Actually, observations repeated after two months showed that the vacancies tend to align parallel to one or two <1$\bar{2}$1> directions, whereas after one year the forbidden 110-type reflections also appeared, indicating that the vacancies are fully ordered.

Acknowledgements

The authors gratefully thank Noémi Szász and Dr. Sandra Drev for sample preparations and Dr. Vincenzo Montedoro at the University of Parma for his support in MOVPE deposition and X-ray characterisation. The research was funded by the National Research, Development and Innovation Fund (NKFIA) via the TÉT_16-1-2016-0025 project (Hungary) and by ARRS, Slovenia (project no. BI-HU/17-18-003). This work is supported also by the project VEKOP-2.3.3-15-2016-00002 of the European Structural and Investment Funds.

References

[1] R. Roy, V. G. Hill, E. F. Osborn, Polymorphism of Ga_2O_3 and the System Ga_2O_3—H_2O, J. Am. Chem. Soc. 74(3) (1952) 719–722.
[2] S. Yoshioka, H. Hayashi, A. Kuwabara, F. Oba, K. Matsunaga, I. Tanaka, Structures and energetics of Ga_2O_3 polymorphs, J. Phys.: Condens. Matter 19(34) (2007) 346211.
[3] A. Hideo, N. Kengo, T. Hidetoshi, A. Natsuko, S. Kazuhiko, Y. Yoichi, Growth of β- Ga_2O_3 Single Crystals by the Edge-Defined, Film Fed Growth Method, Jpn. J. Appl. Phys. 47 (2008) 8506-8509.
[4] N. M. Sbrockey, T. Salagaj, E. Coleman, G. S. Tompa, Y. Moon, M. S. Kim, Large-area MOCVD growth of Ga_2O_3 in a rotating disc reactor, J. Electron. Mater. 44(5) (2015) 1357-1360.
[5] G. Wagner, M. Baldini, D. Gogova, M. Schmidbauer, R. Schewski, M. Albrecht, Z. Galazka, D. Klimm, R. Fornari, Homoepitaxial growth of β-Ga_2O_3 layers by metal-organic vapor phaseepitaxy, Phys. Status Solidi Appl. Mater. Sci. 211(1) (2014) 27-33.
[6] W. Mi, J. Ma, C. Luan, H. Xiao, Structural and optical properties of β-Ga_2O_3 films depositedon $MgAl_2O_4$ (100) substrates by metal–organic chemical vapor deposition, J. Lumin. 146(8) (2014) 1–5.
[7] M. Baldini, M. Albrecht, A. Fiedler, K. Irmscher, D. Klimm, R. Schewski, G. Wagner, Semiconducting Sn-doped β-Ga_2O_3 homoepitaxial layers grown bymetal organic vapour-phase epitaxy, J. Mater. Sci. 51 (7) (2016) 3650–3656.
[8] M. J. Tadjer, M. A. Mastro, N. A. Mahadik, M. Currie, V. D. Wheeler, J. A. Freitas Jr., J. D. Greenlee, J. K. Hite, K. D. Hobart, C. R. Eddy Jr., F. J. Kub, Structural, optical, and electrical characterization of monoclinic β-Ga_2O_3 grown by MOVPE on sapphire substrates, J. Electron. Mater. 45(4) (2016) 2031–2037.
[9] V. Gottschalch, K. Mergenthaler, G. Wagner, J. Bauer, H. Paetzelt, C. Sturm, U. Teschner, Growth of β-Ga_2O_3 on Al_2O_3 and GaAs using metal-organic vapour phase epitaxy, Phys. Status Solidi 206(2) (2009) 243–249.
[10] D. Gogova, M. Schmidbauer, A. Kwasniewski, Homo- and heteroepitaxial growth of Sn-doped β-Ga_2O_3 layers by MOVPE, Cryst. Eng. Comm. 17(35) (2015) 6744–6752.
[11] S. Rafique, L. Han, M. J. Tadjer, J. A. Freitas, N. A. Mahadik, H. Zhao, Homoepitaxial growth of β-Ga_2O_3 thin films by low pressure chemical vapor deposition, Appl. Phys. Lett. 108(18) (2016) 182105.
[12] M. Handwerg, R. Mitdank, Z. Galazka, S. F. Fischer, Temperature-dependent thermal conductivity in Mg-doped and undoped β-Ga_2O_3 bulk-crystals, Semicond. Sci. Technol. 30(2) (2015) 24006.

[13] M. Baldini, M. Albrecht, A. Fiedler, K. Irmscher, R. Schewski, G. Wagner, Si- and Sn-doped homoepitaxial β-Ga_2O_3 layers grown by MOVPE on (010)-oriented substrates, ECS J. Solid State Sci. Technol. 6(2) (2017) Q3040–Q3044.
[14] M. Higashiwaki, K. Sasaki, A. Kuramata, T. Masui, S. Yamakoshi, Development of gallium oxide power devices, Phys. Status Solidi Appl. Mater. Sci. 211 (2014) 21-26.
[15] W. S. Hwang, A. Verma, H. Peelaers, V. Protasenko, S. Rouvimov, H. Xing, A. Seabaugh, W. Haensch, C. Van de Walle, Z. Galazka, M. Albrecht, R. Fornari, D. Jena, High-voltage field effect transistors with wide-bandgap β-Ga_2O_3 nanomembranes, Appl. Phys. Lett. 104 (2014) 249902.
[16] S. Nakagomi, T. Momo, S. Takahashi, Y. Kokubun, Deep ultraviolet photodiodesbased on β-Ga_2O_3/SiC heterojunction, Appl. Phys. Lett. 103 (2013) 72105.
[17] T. Oshima, T. Okuno, N. Arai, N. Suzuki, H. Hino, S. Fujita, Flame detection by a β-Ga_2O_3-based sensor, Jpn. J. Appl. Phys. 48 (2009) 011605.
[18] X. Z. Liu, P. Guo, T. Sheng, L. X. Qian, W. L. Zhang, Y. R. Li, β-Ga_2O_3 thin films on sapphire pre-seeded by homo-self-templated buffer layer for solar-blind UV photodetector, Opt. Mater. (Amst) 51 (2016) 203-207.
[19] M. Pavesi, F. Fabbri, F. Boschi, G. Piacentini, A. Baraldi, M. Bosi, E. Gombia, A. Parisini, R. Fornari, The electronic structure of ε-Ga_2O_3, Mater. Chem. Phys. 205 (2018) 502–507.
[20] I. Levin, D. Brandon, Metastable Alumina Polymorphs: Crystal Structures and Transition Sequences, J. Am. Ceram. Soc. 81 (2005) 1995–2012.
[21] S. Geller, Crystal Structure of β- Ga_2O_3, J. Chem. Phys. 33 (1960) 676–684.
[22] S. Geller, On the structure of β- β- Ga_2O_3, J . Solid State Chem. 20 (1977) 209–210.
[23] J. Åhman, G. Svensson, J. Albertsson, A Reinvestigation of β-Gallium Oxide, Acta Cryst. C 52 (1996) 1336–1338.
[24] T. Sato, T. Nakamura, Thermal decomposition of gallium hydroxides, Thermochim. Acta 53 (1982) 281–288.
[25] L. A. O'Dell, S. L. P. Savin, A. V. Chadwick, M. E. Smith, Multinuclear MAS NMR investigation of sol-gel and ball-milled nanocrystalline Ga_2O_3, Appl. Magn. Reson. 32 (2007) 527–546.
[26] H. Y. He, M. A. Blanco, R. Pandey, Electronic and Thermodynamic Properties of β-Ga_2O_3, Appl. Phys. Lett. 88 (2006) 261904.
[27] H. Y. Playford, A. C. Hannon, E. R. Barney, R. I. Walton, Structures of Uncharacterised Polymorphs of Gallium Oxide from Total Neutron Diffraction. Chem. - Eur. J. 19 (2013) 2803−2813.
[28] I. Cora, F. Mezzadri, F. Boschi, M. Bosi, M. Caplovicova, G. Calestani, I. Dódony, B. Pécz, R. Fornari, The real structure of ε-Ga_2O_3 and its relation to κ-phase, Cryst. Eng. Comm. 19 (2017) 1509-1516.
[29] W. H. Zachariasen, Skrifter utgitt av det Norske Videnskaps-Akademi i Oslo 1: Matematisk-Naturvidenskapelig Klasse 4 (1928) 6–166.
[30] S. I. Stepanov, V. I. Nikolaev, V. E. Bougrov, A. E. Romanov, Gallium Oxide: Properties and Applications - a Review. Rev. Adv.Mater. Sci. 44 (2016) 63−86.
[31] Y. Xu, J.-H. Park, Z. Yao, C. Wolverton, M. R., J. Wu, V. P. Dravid, Strain-Induced Metastable Phase Stabilization in Ga_2O_3 Thin Films, ACS Appl. Mater. Interfaces 11 (2019) 5536−5543.
[32] K. Shimada, First-principles study of crystal structure, elastic stiffness constants, piezoelectric constants, and spontaneous polarization of orthorhombic $Pna2_1$–M_2O_3 (M = Al, Ga, In, Sc, Y), Mater. Res. Express 5 (2018) 036502.
[33] J. Kim, D. Tahara, Y. Miura, B. G. Kim, First-principle calculations of electronic structures and polar properties of (κ,ε)-Ga_2O_3, Appl. Phys.Express 11 (2018) 061101.
[34] M. B. Maccioni, V. Fiorentini, Phase diagram and polarization of stable phases of $(Ga_{1-x}In_x)_2O_3$, Appl. Phys. Express 9 (2016) 041102.
[35] F. Mezzadri, G. Calestani, F. Boschi, D. Delmonte, M. Bosi, R. Fornari, Crystal Structure and Ferroelectric Properties of ε-Ga_2O_3 Films Grown on (0001)-Sapphire, Inorg. Chem. 55 (2016) 12079–12084.
[36] G. Eranna, B. C. Joshi, D. P. Runthala, R. P. Gupta, Oxide Materials for Development of Integrated Gas Sensors – A Comprehensive Review. Crit. Rev. Solid State Sci. 29 (2004) 111−188.
[37] Y. Oshima, E. G. Víllora, Y. Matsushita, S. Yamamoto, K. Shimamura, Epitaxial growth of phase-pure ε-Ga_2O_3 by halide vapor phase epitaxy, J. Appl. Phys. 118 (2015) 085301.
[38] F. Boschi, M. Bosi, T. Berzina, E. Buffagni, C. Ferrari, R. Fornari, Hetero-epitaxy of ε-Ga_2O_3 layers by MOCVD and ALD, J. Cryst.Growth 443 (2016) 25-30.
[39] X. Xia, Y. Chen, Q. Feng, H. Liang, P. Tao, M. Xu, G. Du, Hexagonal phase-pure wide band gap ε-Ga_2O_3 films grown on 6H-SiC substrates by metal organic chemical vapor deposition, Appl. Phys. Lett. 108 (2016) 202103.
[40] A. Parisini, A. Bosio, V. Montedoro, A. Gorreri, A. Lamperti, M. Bosi, G. Garulli, S. Vantaggio, R. Fornari, Si and Sn doping of ε-Ga_2O_3 layers, APL Mater. 7 (2019) 031114.
[41] M. Kneiß, A. Hassa, D. Splith, C. Sturm, H. von Wenckstern, T. Schultz, N. Koch, M. Lorenz, M. Grundmann, Tin-assisted heteroepitaxial PLD-growth of κ-Ga_2O_3 thin films with high crystalline quality, APL Mater. **7** (2019) 022516.
[42] A. Hassa, H. von Wenckstern, D. Splith, C. Sturm, M. Kneiß, V. Prozheeva, M. Grundmann, Structural, optical, and electrical properties of orthorhombic κ-$(In_xGa_{1-x})_2O_3$ thin films, APL Mater. 7 (2019) 022525.
[43] Y. Chen, X. Xia, H. Liang, Q. Abbas, Y. Liu, G. Du, Growth Pressure Controlled Nucleation Epitaxy of Pure Phase ε- and β-Ga_2O_3 Films on Al_2O_3 via Metal-Organic Chemical Vapor Deposition, Cryst. Growth Des. 18 (2018) 1147−1154.
[44] H. Sun, K.-H. Li, C. G. T. Castanedo, S. Okur, G. S. Tompa, T. Salagaj, S. Lopatin, A. Genovese, X. Li, HCl Flow-Induced Phase Change of α-, β-, and ε-Ga_2O_3 Films Grown by MOCVD, Cryst. Growth Des. 18 (2018) 2370−2376.
[45] M. Mulazzi, F. Reichmann, A. Becker, W. M. Klesse, P. Alippi, V. Fiorentini, A. Parisini, M. Bosi, R. Fornari, The electronic structure of ε-Ga_2O_3, APL Mater. 7 (2019) 022522.
[46] R. Fornari, M. Pavesi, V. Montedoro, D. Klimm, F. Mezzadri, I. Cora, B. Pécz, F. Boschi, A. Parisini, A. Baraldi, C. Ferrari, E. Gombia, Thermal stability of ε-Ga_2O_3 polymorph, Acta Materialia 140 (2017) 411-416.
[47] A. Barna, G. Radnóczi, B. Pécz, Handbook of Microscopy, in: Handb. Microsc., S. Amelinc, VCH Verlag, 1997: p. 751.
[48] P. A. Stadelmann, JEMS, (n.d.), http://www.jems-saas.ch/Home/jemsWebSite/jems.html.
[49] C. Li, G. Habler, T. Griffiths, A. Rečnik, P. Jeřábek, L. C. Götze,C. Mangler, T. J. Pennycook, J. Meyer, R. Abarta, Structure evolution of h.c.p./c.c.p. metal oxide interfaces in solid-state reactions, Acta Cryst. A74 (2018) 1-15.
[50] H. Y. Playford, A. C. Hannon, M.G. Tucker, D. M. Dawson, S.E. Ashbrook, R. J. Kastiban, J. Sloan, R. I. Walton, Characterization of Structural Disorder in γ-Ga2O3, J. of Physical Chemistry C 118(29) (2014) 16188-16198.
[51] K. Pohl, Hydrothermale Bildung von γ-Ga_2O_3, Naturwissenschaften 55 (1968) 82-82.
[52] M. Zinkevich, F. M. Morales, H. Nitsche, M. Ahrens, M. Ruehle, F. Aldinger, Microstructural and thermodynamic study of γ-Ga_2O_3, Zeitschrift für Metallkunde 95(9) (2004) 756-762.
[53] L. Deyu, B. H. O'Connor, G. I. D. Roach, J. B. Cornell, Structural models of eta- and gamma-aluminas by X-ray Rietveld refinement, Acta Cryst. A 46 (1990) C61.

[54] G. Gutierrez, A. Taga, B. Johansson, Theoretical structure determination of γ−Al_2O_3, Physical Review B - Condensed Matter 65(1) (2002) 012101.
[55] V. Saraswati, G.V.N. Rao, X-ray diffraction in γ-alumina whiskers, J. of Cryst. Growth 83 (1987) 606-609.
[56] W. Guse, H. Saalfeld, X-ray characterization and structure refinement of a new cubic alumina phase (sigma-Al_2O_3) with spinel-type structure, Neues Jahrbuch für Mineralogie 5 (1990) 217-226.

Name	Sample type	Annealing	Heating ramp1	Heating ramp2	Transformation temp.	Result
Sample#1	plan view	*in situ* in vacuum	0-1000°C with 2°C/min		~950-960°C	κ→β and after cooling γ appeared
Sample#2	cross sect.	*in situ* in vacuum	0-600°C with 50°C/5min	600°C< with 5°C/min	~980°C	κ→β and after cooling γ appeared
Sample#3	cross sect.	*in situ* in vacuum	0-600°C with 50°C/5min	600°C< with 3°C/min	~980°C	κ→β and after cooling γ appeared
Sample#4	cross sect.	*in situ* in vacuum	0-500°C with 50°C/5min	500-850°C with 1°C/min 850°C< with 1°C/min with keeping the sample at a fixed temperature for 10 min at intervals of 20°C	~950°C	κ→β and after cooling γ appeared
Sample#5	cross sect.	*ex situ* in ambient air	0-500°C with 50°C/5min	500-820°C with 10°C/min and with keeping the sample at 820°C for 15 min	not above 820°C	κ→γ with no β

Table 1: List of samples with details of the experiments.

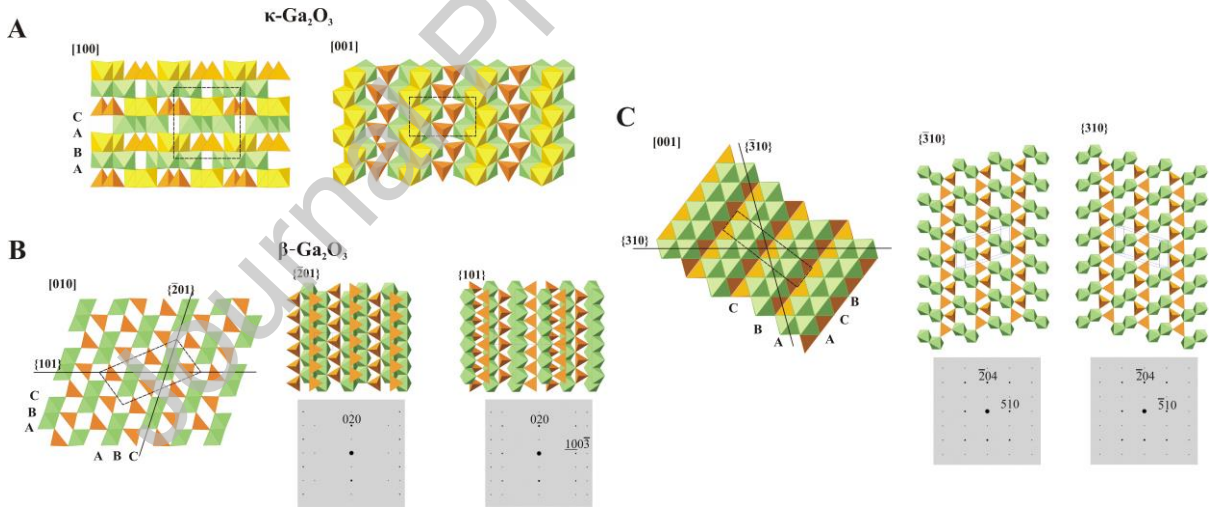

Figure 1. (A) The polyhedral representation (Ga atom in the centre and 6 or 4 O atoms in the corners of the polyhedral, *i.e.* octahedral or tetrahedra) of orthorhombic κ- Ga_2O_3. from [100] and [001] zone axis. It has a 4H (ABAC) oxygen sublattice with two types of polyhedral layer (*i.e.* pure octahedral and a mixed (octahedral + tetrahedral) layer). **(B)** and **(C)** the polyhedral representation of the monoclinic β-phase. 2-2 polyhedral layers cut from [010] **(B)** and [001] **(C)** projections, parallel to {$\bar{2}$01},{101} and {$\bar{3}$10},{310}, respectively, with

projections of reciprocal lattices show the 4 types of close-packed layers (since oxygen sublattice has a *ccp* stacking).

OR1	$\{001\}_{\alpha\text{-}Al2O3} \parallel \{001\}_{\kappa\text{-}Ga2O3} \parallel \{2\text{-}01\},\{101\},\{31\text{-}0\},\{310\}_{\beta\text{-}Ga2O3}$
OR2	$[001]_{\kappa}\ \{010\}_{\kappa} \parallel [2\underline{1}01]_{\beta}\ \{2\text{-}04\}_{\beta}$
OR3	$[001]_{\kappa}\ \{010\}_{\kappa} \parallel [2\underline{1}01]_{\beta}\ \{2\text{-}04\}_{\beta} \parallel [11\text{-}1]_{\gamma}\ \{220\}_{\gamma}$ $[001]_{\kappa}\ \{100\}_{\kappa} \parallel [2\underline{1}01]_{\beta}\ \{510\}_{\beta} \parallel [11\text{-}1]_{\gamma}\ \{22\text{-}4\}_{\gamma}$
OR4	$[001]_{\kappa}\ \{001\}_{\kappa} \parallel [2\text{-}\underline{1}01\text{-}]_{\beta1}\ \{31\text{-}0\}_{\beta1} \parallel [2\underline{1}01]_{\beta2}\ \{310\}_{\beta2}$

Table 2. List of orientation relationships between the polymorphs.

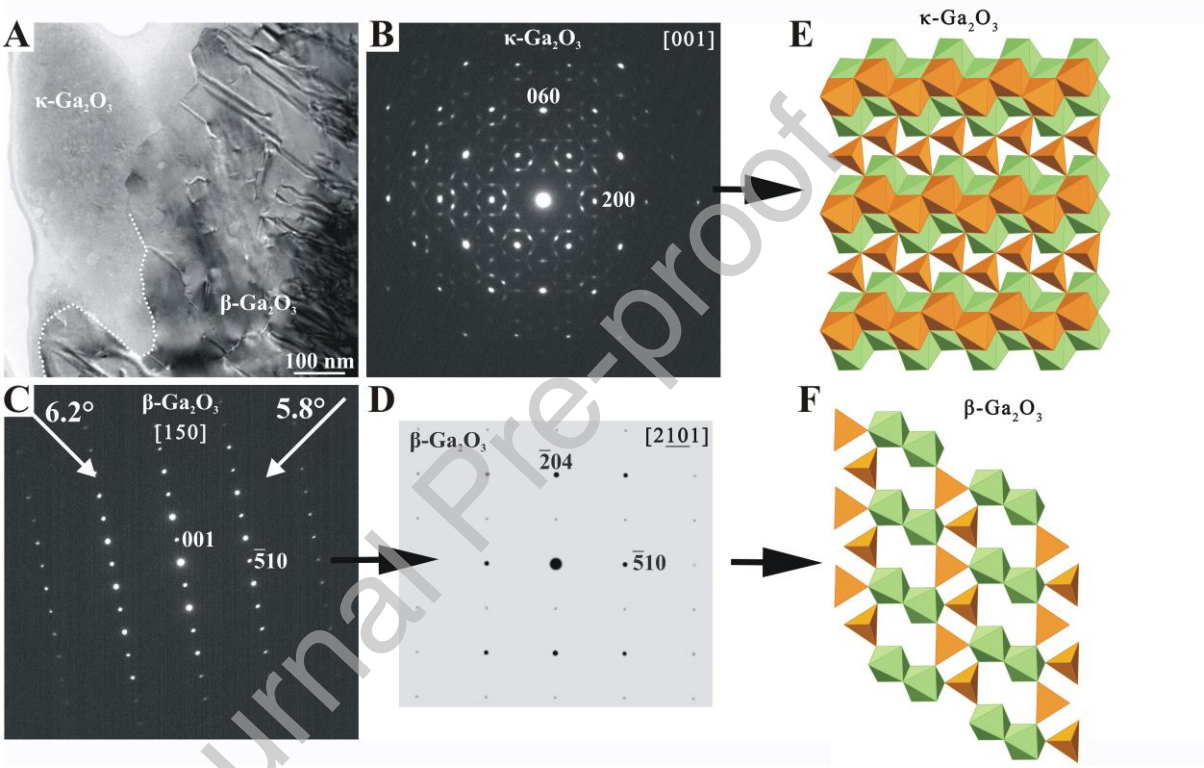

Figure 2. BF-TEM image (**A**) of sample #1 shows the interface between κ and β at 950°C in $[001]_{\kappa}$ projection (*i.e.* $[2\underline{1}01]_{\beta}$ projection). (**B**) shows the [001] projected SAED pattern of the κ-phase. Since it is a high index zone for the β-phase, we tilted it to the closest low index zone axis. (**C**) shows the SAED pattern of β-phase after tilting the sample for Δx=+6.2° and Δy=+5.8°. From these the original orientation of β-phase could be reconstructed (**D**) and that can reveals the following orientation relationship (OR2, **Table 2**): $[2\underline{1}01]_{\beta}\ \{\bar{2}04\}_{\beta} \parallel [001]_{\kappa}\ \{010\}_{\kappa}$, *i.e.* $\{310\}_{\beta}$ plane (**F**) is parallel to $\{001\}_{\kappa}$ (**E**).

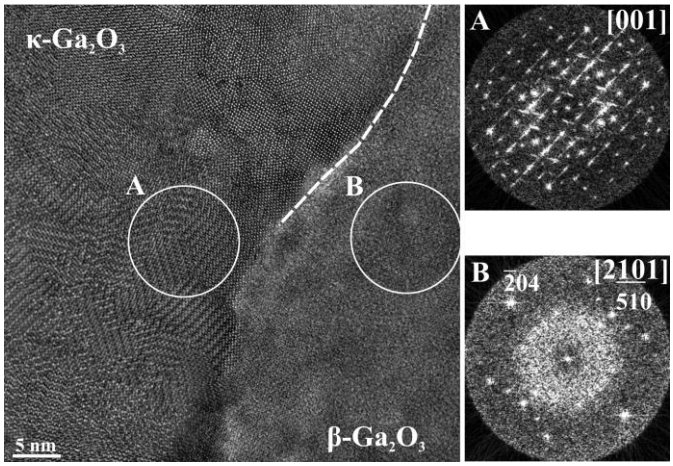

Figure 3. HRTEM image of sample #1 in [001] projection for the κ-phase shows the interface between the κ and β grains after transformation. FFT images of κ- (**A**) and β-phase (**B**) from the signed area on the HRTEM confirm the orientation and structural relationship OR2 (**Table 2**), *i.e.*: $[2\underline{1}01]_{\beta}\ \{\bar{2}04\}_{\beta} \parallel [001]_{\kappa}\ \{010\}_{\kappa}$.

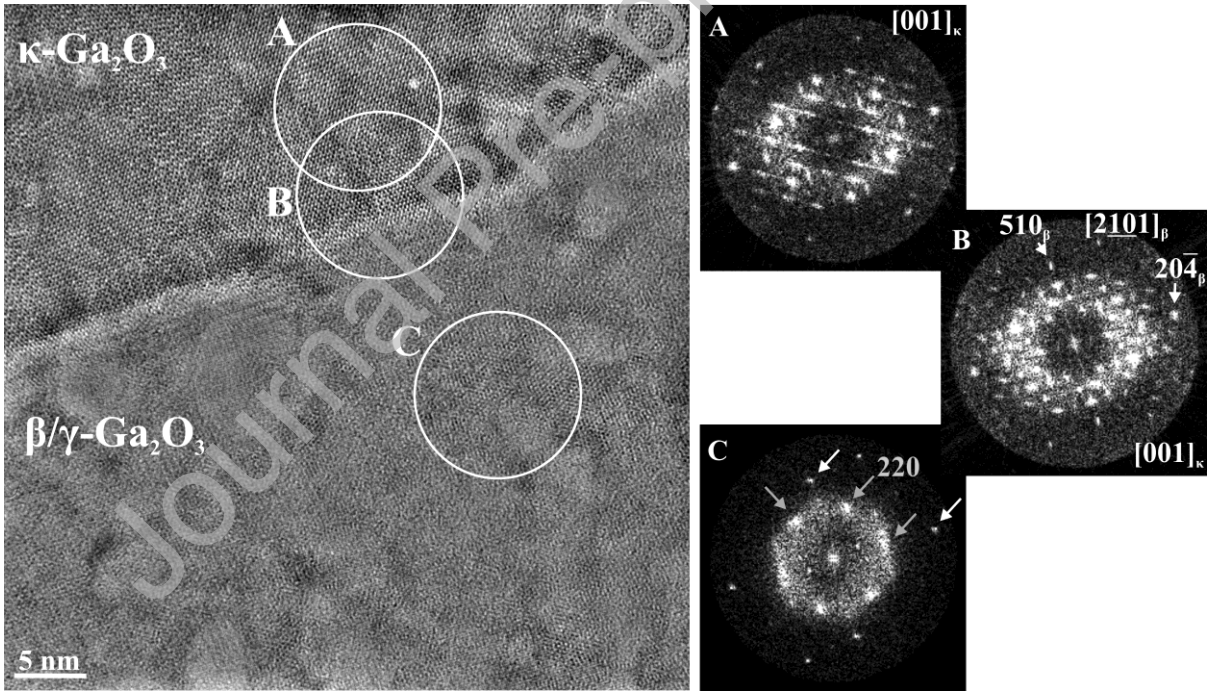

Figure 4. HRTEM image of sample #1 from the κ/β interface in [001] projection of the κ-phase. **A**, **B** and **C** are FFT images calculated from the marked areas on HRTEM. FFT from area C shows three reflections at 2.5 Å on every 60° (grey arrows), that could correspond to the 220-type reflections in $[1\bar{1}1]$ zone axis of the γ-phase, since *ccp* stacking of O-sublattice in γ-phase is parallel to the <111> directions and that would correspond to those of κ-phase in [001] projection. Honeycomb-like patterns on HRTEM support this presumption. Orientation

relationship (OR3, **Table 2**) between the 3 phases are as follows: $[001]_{\kappa}$ $\{100\}_{\kappa}$ || $[2\underline{1}0\underline{1}]_{\beta}$ $\{510\}_{\beta}$ || $[1\bar{1}1]_{\gamma}$ $\{2\bar{2}4\}_{\gamma}$.

Video 1. All samples were heated up to 600°C in larger steps (50°C/5 min), then we applied 3°C/min heating ramp in sample #3. We observed phase transformations at 980°C. Transformation suddenly started and was very quick, but the transformation could be recorded in real time at 20K magnification. The new phase nucleated in the thicker part of the sample then it expanded in lateral direction up to the middle of the observation field. The new phase was identified as the thermodynamically stable β-phase.

Video 2 and Video 3. We repeated the same experiment with sample #4, applying the slowest heating ramp. After 500 °C the heating rate was 1°C/min, while above 850°C we kept the sample at a fixed temperature for 10 minutes at intervals of 20°C. The transformation started at about 950°C, but it was slower than observed in sample #3, presumably because of the lower heating speed that did not generate any temperature overshooting by the temperature controller. The transformation started in the middle of the layer as well, and spread laterally, self-sustained by the exothermic heat.

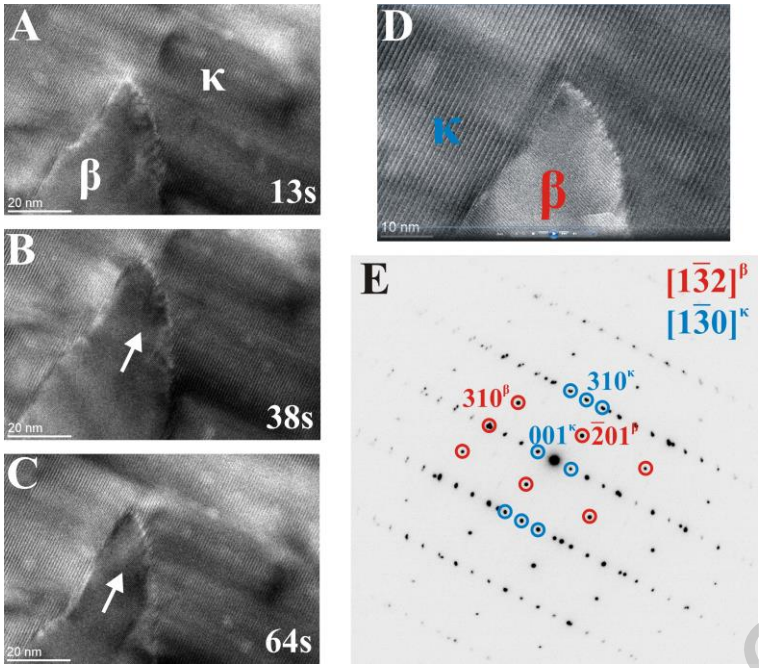

Figure 5. (**A**), (**B**) and (**C**) are shots from video 2 (sample #4) which show the lateral propagation of the β-phase at 960°C. (**D**) is another shot from video3 at higher magnification showing the orientation relationships between β and κ, that are consistent with the acquired SAED pattern (**E**).

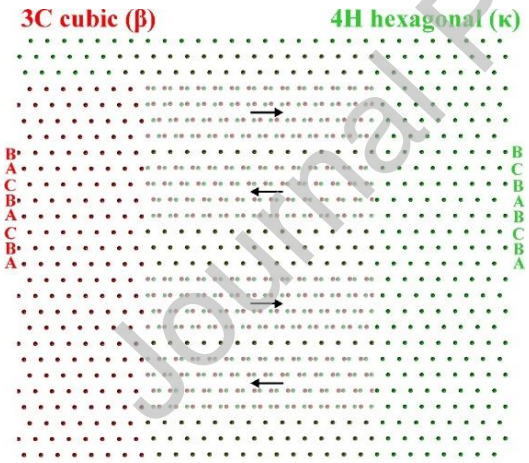

Figure 6. During the transformation oxygen layers are reconstructed from 4H (ABCB) *hcp* (right) to 3C *ccp* (ABC) (left); 4 layers out of the 12 run undisturbed across the two phases.

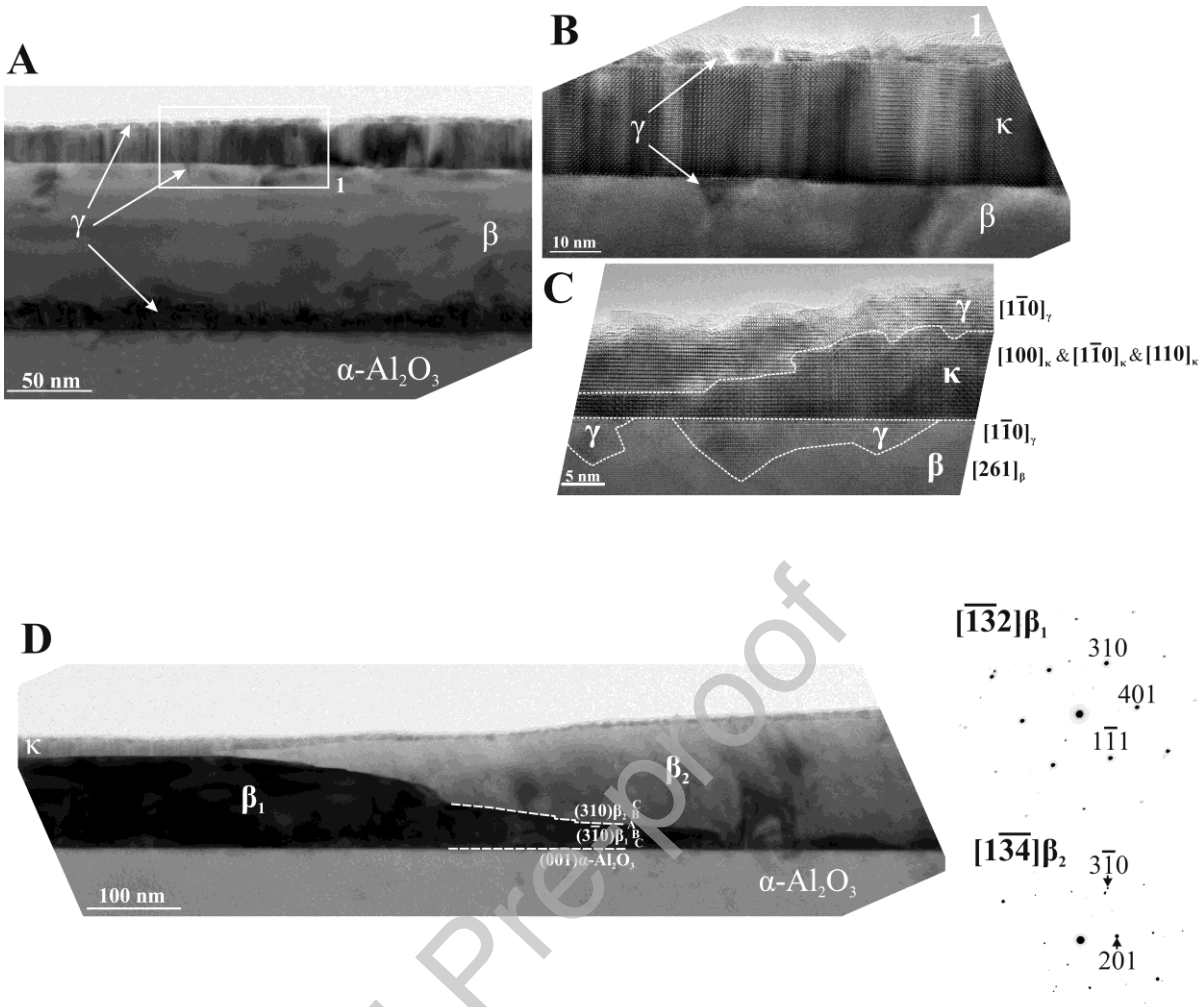

Figure 7. TEM cross-sections of κ→β transition from sample #2**.** BF-TEM image (**A**), where β almost entirely took over the κ epilayers. Thin κ-phase remained untransformed at the interface with sapphire substrate and on the very top of the epilayers (see also **B and C**). Traces of the cubic γ-phase were found at the interface between κ and β, as well on the uppermost film surface. It seems it formed when the transitions slows down and goes to termination. The OR3 (**Table 2**) is the following: $[001]_{\kappa}$ $\{100\}_{\kappa}$ || $[2\underline{10}1]_{\beta}$ $\{510\}_{\beta}$ || $[1\bar{1}1]_{\gamma}$ $\{2\bar{2}4\}_{\gamma}$.

BF image with the two SAED patterns **(D)** from different region of the sample shows two differently oriented β-domains obtained after conversion of the κ epilayer. The orientation relationship between them are the following OR4 (**Table 2**): $[001]_{\kappa}$ $\{001\}_{\kappa}$ || $[\bar{2}\underline{10}\bar{1}]_{\beta1}$ $\{3\bar{1}0\}_{\beta1}$ || $[2\underline{10}1]_{\beta2}$ $\{310\}_{\beta2}$. The stacking direction of close-packing oxygen sheets is the opposite for the two grains.

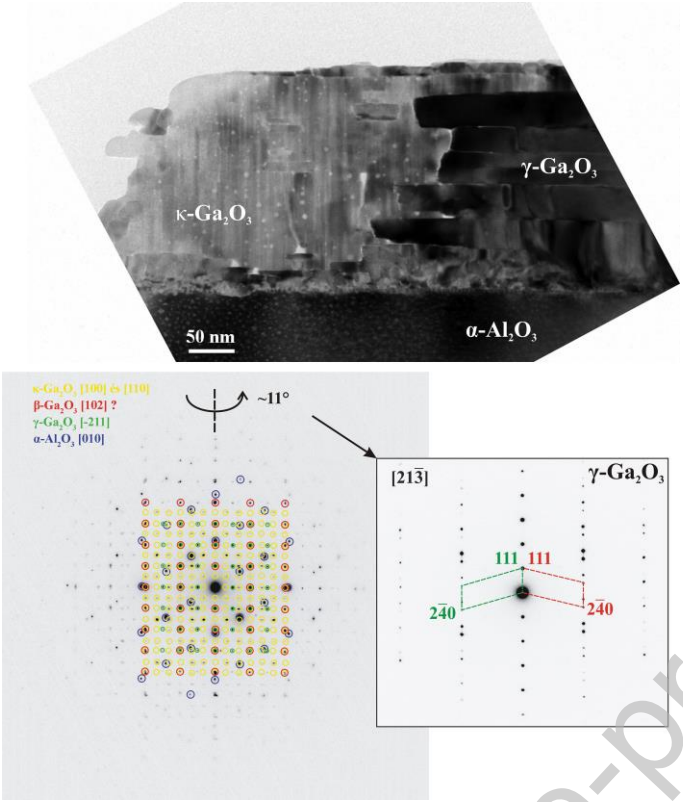

Figure 8. Partial transformation observed in the sample#5 annealed *ex situ* up to 820°C. The converted region was identified as cubic γ-phase from diffraction patterns. This phase first appears in the mid of the layer. In the thicker part the phase consists of ca. 50 nm wide elongated slabs. Tilting the sample into $[21\bar{3}]_\gamma$ projection reveals {111} twinning of γ-phase. Round shape regions showing whiter contrast could be holes growing after the annealing process in TEM generated after the movement of twin/domain boundaries.

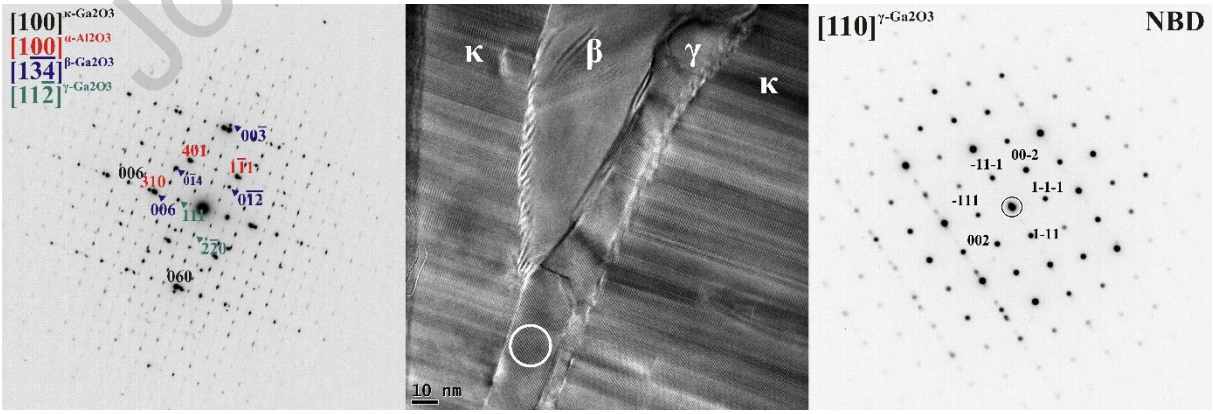

Figure 9. SAED pattern and HRTEM image of the *in-situ* annealed sample#4 and NBD pattern of γ phase from the HRTEM. The approximate size of the beam in nanobeam mode is signed with a white circle in the HRTEM image. Reflection intensities from NBD were compared with the simulated diffraction intensities in [110] zone.

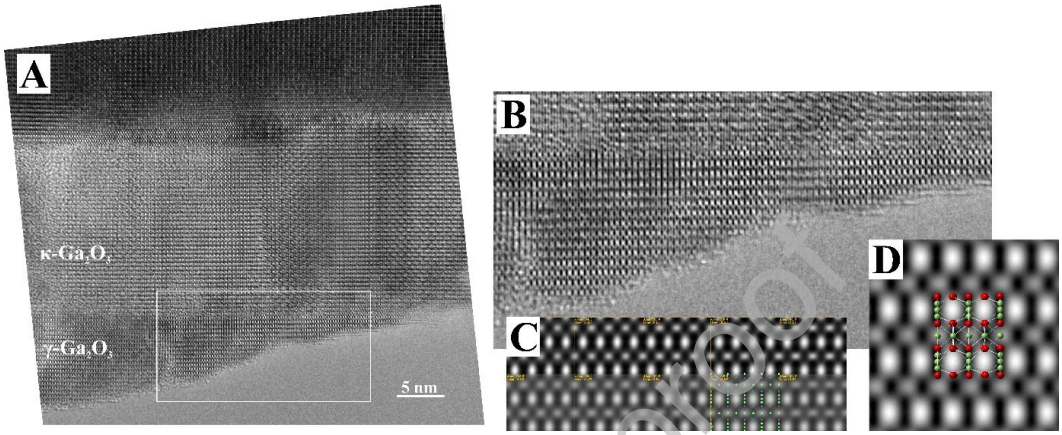

Figure 10. Experimental HRTEM image (**A and B**) of the γ phase from the thinnest part of sample#5 annealed *ex situ* up to 820°C. **D** shows the symmetry averaged experimental HRTEM image in [11-2] zone axis of γ-Ga_2O_3. Multislice simulation (**C**) for *16d* structure using JEMS [48] well agree with the experimental image.

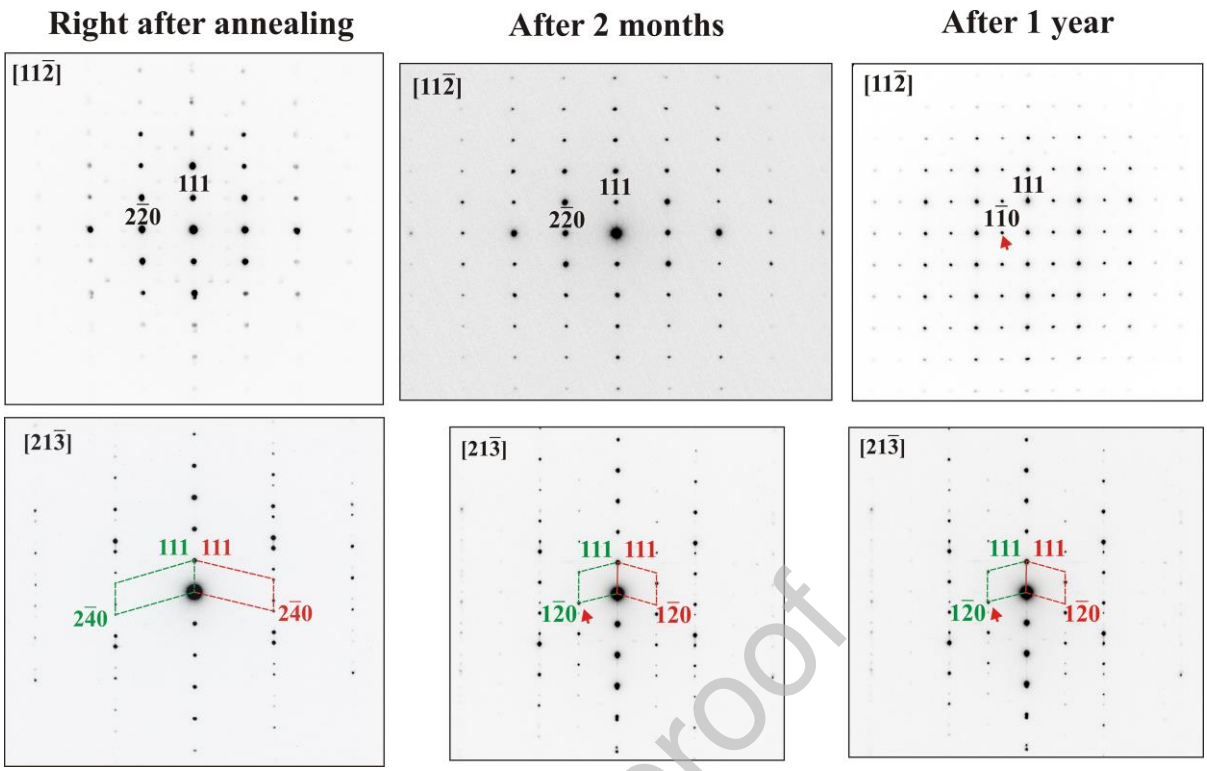

Figure 11. SAED patterns of γ-Ga_2O_3 acquired right after annealing, 2 months after and 1 year after annealing from [11-2] and [21-3] zone axis. After 2 months 1-20 reflection appears, while 1-10 is still forbidden. After 1 year 1-10 reflection also appeared, showing the ongoing ordering process of Ga/vacancy. Very weak extra spots beside spots of γ phase proved to belong to the unconverted κ phase.

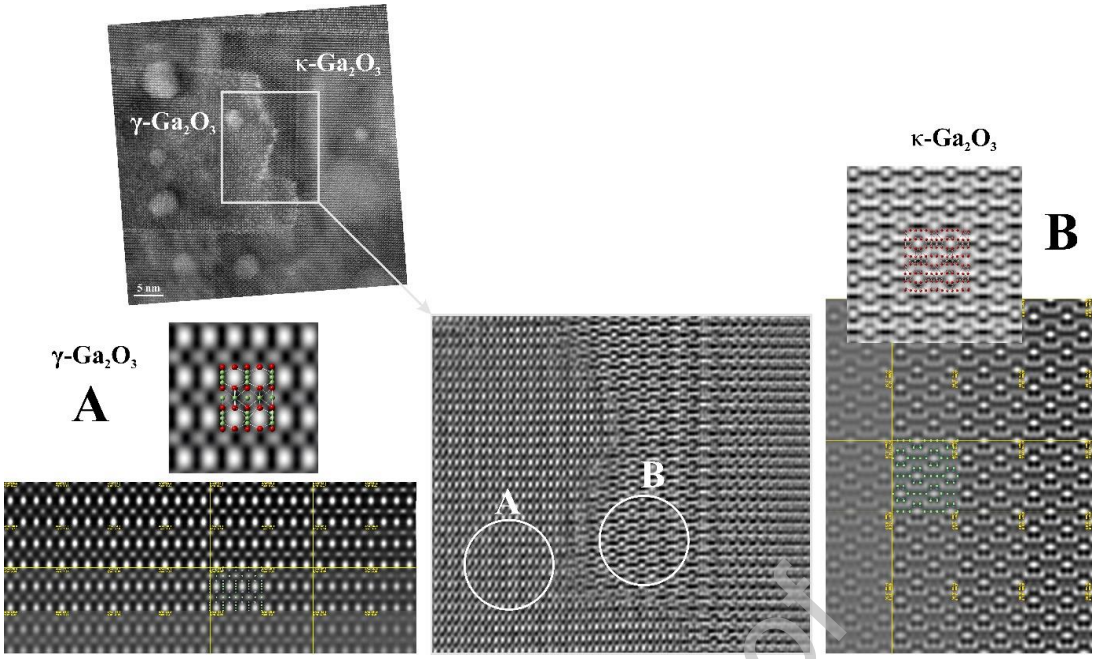

Figure 12. The interface (marked with white rectangle) of the κ→γ transformation on Fourier-filtered experimental HRTEM image from sample#5 annealed *ex situ* up to 820°C. Left from the interface (**A**) the symmetry averaged, filtered HRTEM image of γ phase with a series of simulated images for comparison. They show good conformity. Right from the interface (**B**) is the same but for the κ-Ga_2O_3.

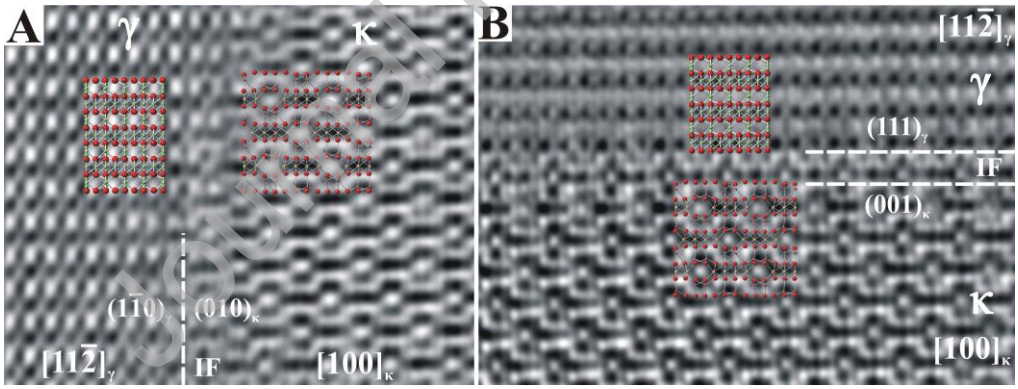

Figure 13. Fourier-filtered experimental HRTEM images of the κ→γ transformation with zig-zag lateral (**A**) and sharp vertical (**B**) interfaces in the thin film from sample#5 annealed *ex situ* up to 820°C. On the zig-zag lateral interface (**A**) the pure octahedral layer of κ phase meets the octahedral kagome layer of γ phase and so do the mixed, tetra-, octahedral layers. On the vertical (**B**) interface there is a 2 monolayers thick transformation zone (1 similar to kagome and a mixed, tetra-, octahedral layer) between the two structure, that differs in structure from γ and κ.

Declaration of interests

The authors declare that they have no known competing financial interests or personal relationships that could have appeared to influence the work reported in this paper.